



LAWRENCE  
LIVERMORE  
NATIONAL  
LABORATORY

UCRL-JRNL-232262

# Initial Study Comparing the Radiating Divertor Behavior in Single-Null and Double-Null Plasmas in DIII-D

T.W. Petrie, N.H. Brooks, M.E. Fenstermacher, M. Groth, A.W. Hyatt, R.C. Isler, C.J. Lasnier, A.W. Leonard, G.D. Porter, M.J. Schaffer, J.G. Watkins, M.R. Wade

June 28, 2007

Proceedings of 34th EPS Conference on Plasma Physics

## **Disclaimer**

---

This document was prepared as an account of work sponsored by an agency of the United States Government. Neither the United States Government nor the University of California nor any of their employees, makes any warranty, express or implied, or assumes any legal liability or responsibility for the accuracy, completeness, or usefulness of any information, apparatus, product, or process disclosed, or represents that its use would not infringe privately owned rights. Reference herein to any specific commercial product, process, or service by trade name, trademark, manufacturer, or otherwise, does not necessarily constitute or imply its endorsement, recommendation, or favoring by the United States Government or the University of California. The views and opinions of authors expressed herein do not necessarily state or reflect those of the United States Government or the University of California, and shall not be used for advertising or product endorsement purposes.

## Initial Study Comparing the Radiating Divertor Behavior in Single-Null and Double-Null Plasmas in DIII-D

T.W. Petrie<sup>1</sup>, N.H. Brooks<sup>1</sup>, M.E. Fenstermacher<sup>2</sup>, M. Groth<sup>2</sup>, A.W. Hyatt<sup>1</sup>, R.C. Isler,<sup>3</sup> C.J. Lasnier<sup>2</sup>, A.W. Leonard<sup>1</sup>, G.D. Porter<sup>2</sup>, M.J. Schaffer<sup>1</sup>, J.G. Watkins<sup>4</sup>, M.R. Wade<sup>1</sup>  
W.P. West<sup>1</sup>, and the DIII-D Team

<sup>1</sup>General Atomics, P.O. Box 85608, San Diego, California 92186-5608, USA

<sup>2</sup>Lawrence Livermore National Laboratory, Livermore, California, USA

<sup>3</sup>Oak Ridge National Laboratory, Oak Ridge, Tennessee, USA

<sup>4</sup>Sandia National Laboratories, Albuquerque, New Mexico, USA

“Puff and pump” radiating divertor scenarios [1,2] were applied to upper SN and DN H-mode plasmas. Under similar operating conditions, argon (Ar) accumulated in the main plasma of single-null (SN) plasmas more rapidly and reached a higher steady-state concentration when the  $\mathbf{B} \times \nabla B$  ion drift direction was toward the divertor than when the  $\mathbf{B} \times \nabla B$  ion drift direction was out of the divertor. The initial rate that Ar accumulated inside double-null (DN) plasmas was more than twice that of comparably-prepared SNs with the same  $\mathbf{B} \times \nabla B$  direction.

One way to reduce power loading at the divertor targets is to “seed” the divertor plasma with impurities that radiatively reduce the conducted power. Studies have shown that the concentration of impurities in the divertor are increased by raising the flow of deuterium ions ( $D^+$ ) into the divertor by a combination of upstream deuterium gas puffing and active particle exhaust at the divertor targets, i.e., puff-and-pump. An enhanced  $D^+$  particle flow toward the divertor targets exerts a frictional drag on impurities, and inhibits their escape from the divertor. A puff-and-pump approach using Ar as the impurity was successfully applied in recent DIII-D experiments to SN plasmas [3] while maintaining good H-mode performance.

Studies on DIII-D and other tokamaks have shown that both the direction of the toroidal magnetic field  $\mathbf{B}_T$  and the degree of magnetic balance between divertors [i.e., the degree to which the plasma shape is considered SN or DN] are important factors in determining recycling and particle pumping [4,5]. It is unclear whether the favorable results of Ref. [3] can be extended to cases with different magnetic balance and/or  $\mathbf{B}_T$  direction. We show in this paper that reversing the direction of  $\mathbf{B}_T$  or altering the divertor magnetic balance *does* have an impact on how plasmas behave under puff-and-pump conditions.

Our study takes advantage of DIII-D’s capabilities to actively pump SN and DN shapes with high-triangularity. In-vessel pumping of deuterium and Ar, shown schematically in Fig. 1, was done by cryopumps located inside the *upper outer* (“plus”), *upper inner* (“minus”), and *lower outer* (dotted) divertor pumping plenums. To increase the ion  $D^+$  flow toward these pumps, deuterium gas was introduced at an outboard location, as shown. Argon was injected directly into the private flux region (PFR) of the upper outer divertor.

Operating parameters for this experiment were: plasma current  $I_p = 1.2$  MA, toroidal field  $\mathbf{B}_T = 1.75$  T (with the capability to run with either toroidal field direction),  $q_{95} \approx 4.3$ , power input  $P_{IN} \approx 6$  MW, line-averaged density  $\bar{n}_e \approx (0.60-0.75) \times 10^{20} \text{ m}^{-3}$  (or  $\bar{n}_e/n_G \approx 0.55-0.70$ ), and  $H_{ITER89P} = 1.7-2.0$  with Type-1 ELMs. Two configurations were considered: SN plasmas biased toward the top of the vessel with a  $dR_{sep} = +1.0$  cm and DN plasmas with  $dR_{sep} = 0$  (Fig. 1). By definition,  $dR_{sep} = (R_L - R_U)$ , where  $R_L$  is the radius at the outer mid-

plane of the lower divertor separatrix and  $R_u$  is the radius at the outer midplane of the upper separatrix flux surface. The  $D_2$  gas puffing rate ( $\Gamma_{D2}$ ) was held at 108 torr  $\ell/s$  for all cases. Deuterium fueling by the neutral beams was  $\approx 13$  torr  $\ell/s$ . Argon was the seeded impurity, as it radiates effectively at the temperatures prevailing in the divertor and pedestal of DIII-D H-mode plasmas and has a relatively short ionization mean free path. Carbon was the dominant intrinsic impurity. It is convenient to relate the direction of  $\mathbf{B}_T$  in terms of the  $\mathbf{B} \times \nabla B$ -ion particle drift direction; we refer to cases where the  $\mathbf{B} \times \nabla B$  direction is toward the *upper* divertor as " $V_{VB\uparrow}$ " and to cases where the  $\mathbf{B} \times \nabla B$  direction is toward the *lower* divertor as " $V_{VB\downarrow}$ ".

Figure 2 compares SN plasmas with  $V_{VB\uparrow}$  and  $V_{VB\downarrow}$  under puff-and-pump conditions. Both  $\Gamma_{D2}$  and the Ar injection rate ( $\Gamma_{Ar}$ ), where  $\Gamma_{Ar} = 0.85$  torr  $\ell/s$  for  $V_{VB\uparrow}$  and 1.0 torr  $\ell/s$  for  $V_{VB\downarrow}$ , were held constant after  $t = 3.0$  s [Fig. 2(a)]. The line-averaged density  $\bar{n}_e$  for  $V_{VB\uparrow}$  was  $\approx 20\%$  higher than  $\bar{n}_e$  for  $V_{VB\downarrow}$  [Fig. 2(b)]. Argon initially accumulated in the main plasma at a higher rate for  $V_{VB\uparrow}$  than for  $V_{VB\downarrow}$ , and reached a steady Ar level that was  $\approx 3\text{-}4$  times greater than that of  $V_{VB\downarrow}$  [Fig. 2(c)]; we consider the relative Ar density  $n_{AR}$ , as proportional to the  $I_{ArXV}/n_e$  signal, where  $I_{ArXV}$  is the intensity of an ARXV line (22.15 nm) with its chordal view through the main plasma. A partial detachment of the inner leg for  $V_{VB\uparrow}$  occurred at  $t \approx 3.3$  s, as seen by a drop in neutral pressure ( $P_{RDP}$ ) inside the upper inner baffle plenum [Fig. 2(d)] and a strong increase in the signal along the bolometer chord passing directly through the X-point [*bolo-Xpt* in Fig. 2(e)]. The total radiated power ( $P_{RAD}$ ) also increased more for  $V_{VB\uparrow}$  [Fig. 2(f)]. More Ar was removed by the upper outer cryopump for  $V_{VB\downarrow}$  than for  $V_{VB\uparrow}$ , as implied by the Ar pressure under the baffle measured by a modified Penning gauge [Fig. 2(g)].

Since Ar removal in the upper divertor changed significantly when the  $\mathbf{B} \times \nabla B$  direction was reversed, the radiated emissivity in the divertor was also distributed differently. The emissivity along the inner divertor leg in the  $V_{VB\uparrow}$  was spread out before detachment but was concentrated near the X-point afterwards [Fig. 3(a,b)]. In contrast, the emissivity for  $V_{VB\downarrow}$  had multiple peaks in the divertor both before and after Ar injection [Fig. 3(c,d)].

ArII (461.0 nm) was monitored in the upper and the lower divertors by several spectrometer channels [Fig. 4(a)]. The U5, U2, and the L4 channels viewed the upper outer divertor target, the upper inner divertor target, and the lower outer target of the secondary divertor, respectively. The Ar presence for  $V_{VB\uparrow}$  was more poloidally distributed than that for  $V_{VB\downarrow}$  [Fig. 4(b)], with higher Ar presence in the *lower* divertor for  $V_{VB\uparrow}$ . From density and temperatures derived from Langmuir probes and following the method discussed in Refs [6,7], the Ar flux at the lower outer target is roughly ten times higher for  $V_{VB\uparrow}$ .

In DN plasmas, radiated power increased first in the divertor *opposite* the  $\mathbf{B} \times \nabla B$  direction. For  $V_{VB\downarrow}$ , the radiated power in the upper divertor showed a clear response to the injected Ar, but *no* radiative response in the lower divertor. For  $V_{VB\uparrow}$ , the radiated power in the upper divertor had *no* radiative response to Ar injection into the private flux region of the upper divertor, but a clear increase in the lower divertor. This was consistent with the

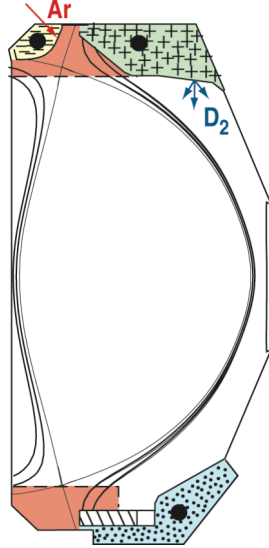


FIG. 1. The poloidal locations of particle pumping- and gas injection are superimposed on the DN plasma cross-sections ( $dR_{sep} = 0$ ) used in this study.

up/down asymmetry in the ArII signals. The presence of Ar in the upper outer divertor (U5) for  $V_{VB\downarrow}$  was higher than that in the lower divertor (L4) [Fig. 4(c)]. This was reversed in  $V_{VB\uparrow}$ . The ratio of Ar flux at the upper outer divertor target to that of the lower outer divertor target was  $\approx 0.4$  for  $V_{VB\uparrow}$  and  $\approx 2.0$  for  $V_{VB\downarrow}$ . For  $V_{VB\downarrow}$ , the ratio of Ar flux at the upper inner divertor target to that of the upper outer target was  $\sim 0.2$ .

Comparison of the puff-and-pump performance between SN and DN shapes shows that the *initial* rate at which the Ar accumulated in the main plasma [ $d(n_{AR})/dt$ ] for the DN was roughly twice the rate for SN with  $V_{VB\downarrow}$  (Fig. 5). Reversing the direction of  $B \times \nabla B$  did little to change the ratio of  $d(n_{AR})/dt$  between the DNs and SNs, i.e., still roughly a factor of 2 for  $V_{VB\uparrow}$ . The rates for  $V_{VB\uparrow}$  were higher than those corresponding to  $V_{VB\downarrow}$ .

The rate of Ar removal by the upper/outer divertor pump was much lower for  $V_{VB\uparrow}$ . More Ar in the  $V_{VB\uparrow}$  case accumulated in the divertor and eventually leaked into the main chamber. Unlike  $V_{VB\downarrow}$ , the inner leg of the  $V_{VB\uparrow}$  plasma detached during Ar injection, enhancing the leakage of Ar. With more Ar in the chamber, Ar accumulated faster in the  $V_{VB\uparrow}$  plasma. Argon accumulated faster in the main plasma of DNs with  $V_{VB\uparrow}$  than with  $V_{VB\downarrow}$ . The fraction of Ar pumped by the upper/outer divertor was

higher for the  $V_{VB\downarrow}$ . As with the SN cases, the Ar leakage out of the upper divertor was greater for  $V_{VB\uparrow}$  than for  $V_{VB\downarrow}$ , and more Ar would be available to “fuel” the main plasma.

Argon accumulated in the divertor of DNs opposite the  $B \times \nabla B$  direction,

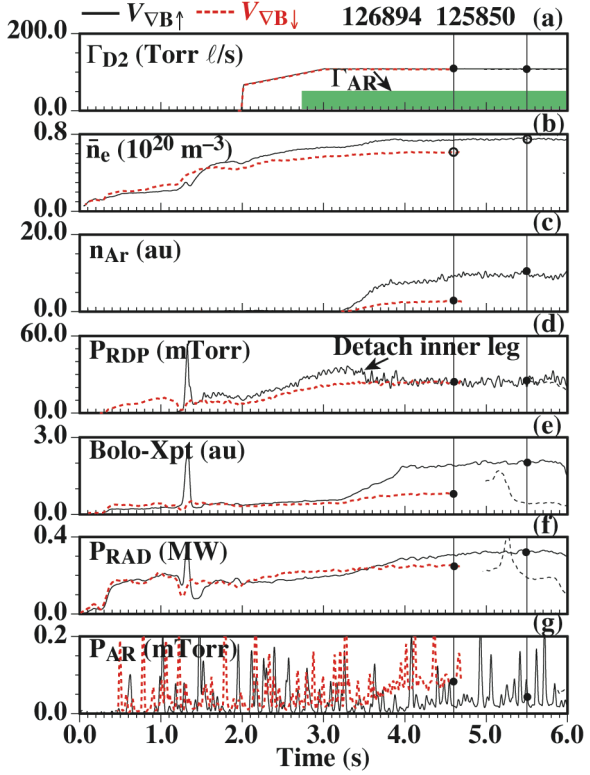


Fig. 2. Two upper SN ( $drsep = +1.0$  cm) H-mode discharges with opposite  $B \times \nabla B$  direction,  $V_{VB\uparrow}$  (solid) and  $V_{VB\downarrow}$  (dashed), are compared. “Steady-state” timeslices are denoted by the vertical lines.

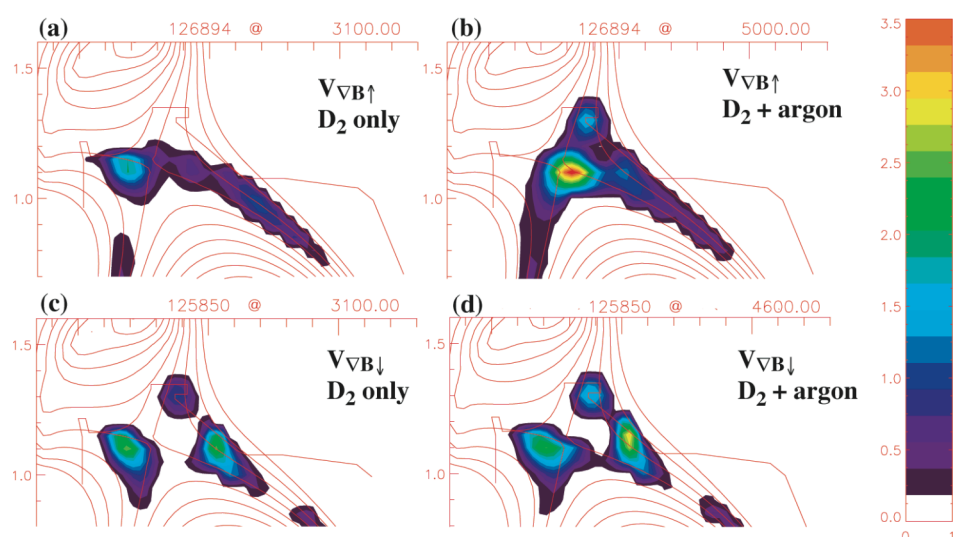


Fig. 3. Tomographic inversions of bolometric arrays are shown for SNs with  $V_{VB\uparrow}$  (a) with deuterium injection only and (b) deuterium and Ar injection together. Also shown are inversions for SNs with  $V_{VB\downarrow}$  (c) deuterium injection only and (d) deuterium and Ar injection together. Only the upper divertor region is shown.

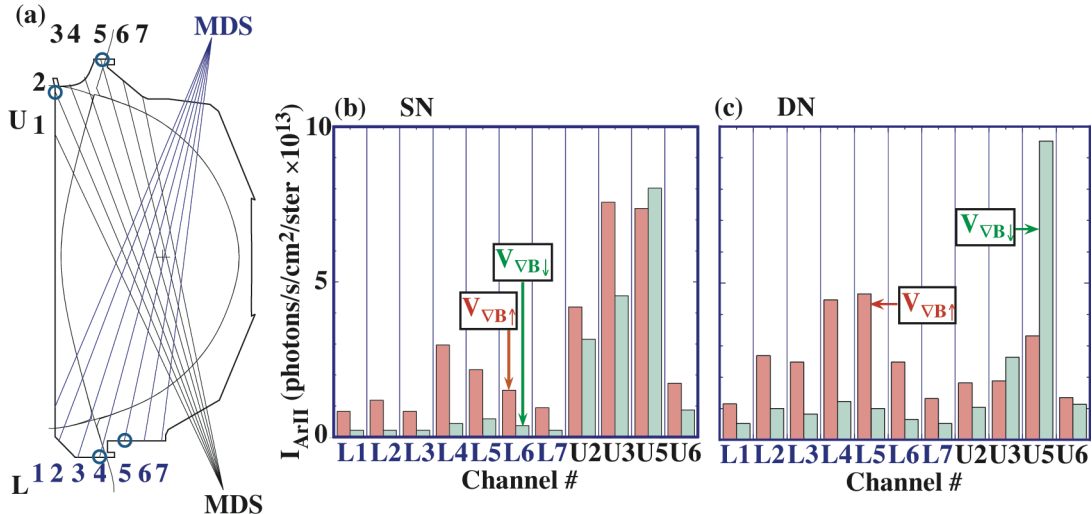


Fig. 4. (a) The chords of the divertor spectrometer that view the upper and lower divertors are superimposed on the DN plasma shape. The ArII signals are shown as a function of view chord designation (b) for the SN cases and (c) for the DN cases discussed in the text.

leading to a greater increase in the radiated power in that divertor over the other divertor. That reversing the direction of  $\mathbf{B}_T$  (or  $\mathbf{B} \times \nabla B$ ) would produce such strikingly different behaviors suggests that particle flows that depend on the direction of the toroidal field may be important. Earlier work in analyzing particle pumping data from DIII-D [6] indicated that the poloidal distribution of neutrals in the divertors (and ultimately the exhaust rates of each pump) was consistent with  $\mathbf{B} \times \nabla B$  and  $E \times B$ -induced particle flows in the divertors and SOL.

Argon accumulation inside DNs was higher than in comparable SNs with the same  $\mathbf{B} \times \nabla B$  direction. A previous study of DIII-D SN and DN plasmas has shown that the characteristic electron temperature for the inboard SOL plasma of the DN is less than that of a comparable SN and that the SOL density profile is narrower for the DN [4]. Because both inner divertor targets of DNs are only tenuously attached (or even detached), it is easier for neutral deuterium (and Ar) to leak into the SOL on the high-field side and then access the main plasma than for the SNs.

This work was performed under the auspices of the U.S. DOE by UC, LLNL under Contract W-7405-Eng-48.

## References

- [1] M.R. Wade, *et al.*, *J. Nucl. Mater.* **266-269** (1999) 44.
- [2] J.A. Goetz, *et al.*, *J. Nucl. Mater.* **266-269** (1999) 359.
- [3] T.W. Petrie, *et al.*, “Compatibility of the Radiating Divertor With High Performance Plasmas in DIII-D,” (to be published in *J. Nucl. Mater.*, 2007).
- [4] T.W. Petrie, *et al.*, *J. Nucl. Mater.* **313-316** (2003) 834.
- [5] T.W. Petrie, *et al.*, *Nucl. Fusion* **46** (2006) 57.
- [6] R.C. Isler, *Nucl. Fusion*, **24** (1984) 1599.
- [7] H.P. Summers, “Atomic Data and Analysis Structure,” JET Joint Undertaking Report JET-IR(94)06, 1994.

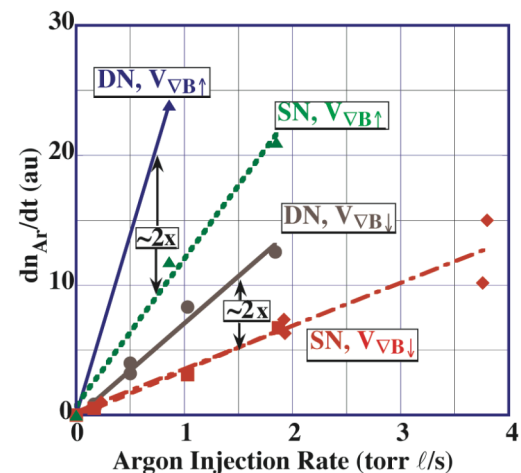


Fig. 5. The initial rate of argon accumulation in SN and DN plasmas is plotted versus  $\Gamma_{\text{Ar}}$  for both  $V_{\text{VB}\downarrow}$  and  $V_{\text{VB}\uparrow}$  cases.